Principal Component Analysis and Blind Separation of Sources for Optical Imaging of Intrinsic Signals

M. Stetter[1], I. Schießl[1], T. Otto[1], F. Sengpiel[2], M. Hübener[2], T. Bonhoeffer[2] and K. Obermayer[1]

[1] **Dept. of Computer Science, Technical University of Berlin, FR2-1, Franklinstraße 28/29, D-10587 Berlin, Germany, http://www.ni.cs.tu-berlin.de/**

[2] **Max Planck Institute of Neurobiology, Am Klopferspitz 18A, D-82152 Munich-Martinsried, Germany, http://www.neuro.mpg.de/**

NeuroImage 2000, in press.

Corresponding author:

Dr. Martin Stetter
Dept. of Computer Science
Technical University of Berlin
FR2-1
Franklinstrasse 28/29
10587 Berlin
Germany

phone: ++49-30-314-73117
fax: ++49-30-314-73121
email: moatl@cs.tu-berlin.de
www: http://www.ni.cs.tu-berlin.de/

Abstract

The analysis of data sets from optical imaging of intrinsic signals requires the separation of signals, which accurately reflect stimulated neuronal activity (mapping signal), from signals related to background activity. Here we show that blind separation of sources by Extended Spatial Decorrelation (ESD) is a powerful method for the extraction of the mapping signal from the total recorded signal. ESD is based on the assumptions, (*i*) that each signal component varies smoothly across space and (*ii*) that every component has zero cross-correlation functions with the other components. In contrast to the standard analysis of optical imaging data, the proposed method (*i*) is applicable to non-orthogonal stimulus-conditions, (*ii*) can remove the global signal, blood-vessel patterns and movement artifacts, (*iii*) works without *ad hoc* assumptions about the data structure in the frequency domain, and (*iv*) provides a confidence measure for the signals (Z-score). We first demonstrate on orientation maps from cat and ferret visual cortex, that Principal Component Analysis (PCA), which acts as a preprocessing step to ESD, can already remove global signals from image stacks, as long as data stacks for at least two – not necessarily orthogonal – stimulus conditions are available. We then show that the full ESD analysis can further reduce global signal components and – finally – concentrate the mapping signal within a single component both for differential image stacks and for image stacks recorded during presentation of a single stimulus.

1 Introduction

Blind Source Separation (BSS) is an emerging signal processing technique, which aims at recovering unobserved signals or 'sources' from a set of observed linear mixtures of these sources. Typically, the mixtures are functions of space or time and are detected by a set of sensors. However, no direct information is available about the sources or about the mixing process, giving rise to the adjective 'blind'. Algorithms for BSS can be regarded as extensions of Principal Component Analysis (PCA), which decorrelates signals and finds directions of extremal variances in the data space. BSS, however, makes additional assumptions about the statistical structure of the sources in order to estimate the separating matrix that recovers the sources from the mixtures. One class of BSS algorithms, which is known as Independent Component Analysis (Jutten and Herault, 1986; Bell and Sejnowski, 1995; Amari, 1996; Cardoso, 1997), is based on the assumption of statistical independence of different sources. A second class of BSS algorithms is based on the assumption of vanishing cross-correlations between sources that are smooth in time (Molgedey and Schuster, 1994). Blind separation of sources has been successfully applied to biomedical data including functional Magnetic Resonance Imaging (fMRI) (McKeown, Makeig, Brown, Jung, McKeown, Makeig, Brown, Jung, Kindermann, Bell and Sejnowski, 1998), electro-encephalograpical measurements (EEG) (Makeig, Bell, Jung and Sejnowski, 1996) and cardiovascular signals (Vetter, Vesin, Celka and Scherrer, 1999).

In this work we demonstrate that PCA and blind separation of sources also provide powerful tools for the statistical analysis of data sets which are obtained from from optical imaging of intrinsic signals (Grinvald, Lieke, Frostig, Gilbert and Wiesel, 1986; Blasdel, 1992). Optical imaging makes use of the fact, that local populations of active neurons cause small changes in the optical properties of the nervous tissue, which can be detected by measuring the light that is reflected back from the neuronal tissue. These evoked changes in the light intensity are called intrinsic signals and can be attributed to several signal components (Bonhoeffer and Grinvald, 1996): (*i*) A component, which reflects stimulated neuronal activity with a high spatial resolution of about 100-200 μm and which is referred to as the "mapping signal". It is related to the deoxygenation of hemoglobin and to local changes in the light scattering properties of the tissue. (*ii*) Global stimulus-related changes in the reflectance with a low spatial resolution and low spatial frequencies, which are referred to as "global signals" and which are dominated by local blood-flow and blood-volume changes. (*iii*) Changes in the reflectance of the larger veins and arteries, denoted as "vessel artifacts". (*iv*) Changes

in optical properties which are uncorrelated to the stimulus (spontaneous neuronal activity (Arieli, Sterkin, Grinvald and Aertsen, 1996), vasomotor response (Mayhew, Askew, Zheng, Porril, Westby, Redgraves, Rector and Harper, 1996)).

The goal of extracting the mapping signal from the measured mixture is often approximated as follows (Bonhoeffer and Grinvald, 1996): First two time-series of images (image stacks) of the brain tissue are recorded for two 'orthogonal' stimulus conditions that are known to excite disjunct neuronal populations. Then the two stacks are subtracted from each other in order to remove the background, and are summed up pixelwise. The resulting image is then bandpass-filtered in order to reduce high-frequency noise and the low-frequency global components. Though being successful in many cases, this procedure suffers from the following drawbacks: (*i*) The global signal and the mapping signal can only be completely separated by bandpass-filtering, if their power spectra do not overlap. However, for the case of ocular dominance and orientation maps, both signals overlap considerably in frequency space. (*ii*) The quality of separation as well as important properties of cortical activity maps depend critically on the arbitrary choice of the high-pass cutoff frequency. An example for this dependence is shown in figure 1. The figure displays the number of singularities (solid line) of the orientation map optically recorded from the visual cortex of a ferret (43d old) as a function of the cutoff-frequency of the high-pass filter. The insets are orientation histograms obtained after analysis without (left) and with (right) highpass filtering. They show, how frequently pixels of a given preferred orientation (in bins of 15 deg) are found within the region of interest of the orientation map. The dash-dotted and dashed lines plot the first and the second Fourier components, respectively, of the orientation histogram as functions of the cutoff-frequency of the high-pass filter. All quantities depend on the choice of the cutoff-frequency for which there is no way to determine a "correct" value.

PCA and BSS make less stringent assumptions about the properties of the individual signal components and can be used for the reliable separation of the mapping-signal from the spatiotemporally varying background even if the corresponding power spectra overlap. In the following we present results obtained by these methods. We show that PCA on a sequence of single condition stacks can be already used for the removal of global signals and time-dependent artifacts. The full ESD analysis improves the extraction of the mapping signal from the mixture and is also applicable to individual image stacks based on a single stimulus.

2 Materials and Methods

2.1 Data collection

Optical imaging of intrinsic signals was performed on area 17 of ferrets and cats. Techniques for surgery and animal preparation have been described in detail elsewhere (Bonhoeffer and Grinvald, 1996; Sengpiel, Gödecke, Strawinski, Hübener, Löwel and Bonhoeffer, 1998). For optical imaging, the cortex was illuminated using bandpass-filtered light of 605 ± 10 nm. Images of intrinsic signals in response to visual stimulation were recorded using a cooled slow-scan CCD-camera (ORA2001, Optical Imaging, Germantown, NY). Stimuli consisted of moving oriented bar gratings. If not specified explicitly, for each trial five frames of 600 ms duration were recorded during each 3 s stimulus presentation, followed by an inter-stimulus interval of 7 seconds, in which the next stimulus was presented stationary. A single-condition image stack was obtained by pixelwise summation of the data stacks from several, usually 16, trials for a single given stimulus type and subtraction of the first frame from the subsequent frames of the resulting stack (first frame analysis). A differential image stack was obtained by recording two sets of images using stimuli, that are known to excite complementary neuron populations (orthogonal stimuli), and subtracting both stacks framewise from each other.

2.2 Data representation

Formally, a typical data structure obtained from optical imaging can be described as a set of N images of the brain surface, which are collected at times $t_n, n = 1, ..., N$. The gray-level of the pixel at location $\mathbf{r} = (x, y), 1 \leq x \leq P_x, 1 \leq y \leq P_y$ within the n-th image is given by $x_{n,\mathbf{r}}$. The $N \times P$ matrix, $P = P_x P_y$, of all pixel values $x_{n,\mathbf{r}}$ describes an image stack and is denoted by $\mathbf{X}$. Its column vectors $\mathbf{x_r} = (x_{1,\mathbf{r}}, ..., x_{N,\mathbf{r}})$ represent the time series of gray values for individual pixels $\mathbf{r}$ and are referred to as pixel time series. For the following theoretical considerations, all images are assumed to have zero mean.

2.3 Principal Component Analysis

Principal Component Analysis finds a set of orthogonal directions within the data space, referred to as principal components, along which the variance of the data assumes extremal values. We identify each data point of the data set with an individual pixel time series, and the whole data set with the

set of all pixel time series of an image stack. Then, PCA can be expected to separate contributions to the pixel time series, which vary strongly over space, from those which vary more weakly. Because the set of all principal components is a complete orthonormal system, the whole data set can be exactly reconstructed from its projections onto all principal components. The key idea for the usage of PCA in source separation is, that the data may be reconstructed using only a subset of principal components, in which the mapping signal is concentrated, whereas principal components which describe global signals and artifacts are left away.

The set of N principal component time series $\mathbf{v}_n$ within the data space and the data variances along these directions can be found as the solutions of the eigenvalue problem

$$\mathbf{GV} = \mathbf{\Lambda V}, \tag{1}$$

where $\mathbf{G}$ is the covariance matrix of the data with elements

$$G_{mn} = \langle x_{m,\mathbf{r}} x_{n,\mathbf{r}} \rangle_{\mathbf{r}} := \frac{1}{P} \sum_{\mathbf{r}} x_{m,\mathbf{r}} x_{n,\mathbf{r}}. \tag{2}$$

The $N \times N$ matrix $\mathbf{V}$ contains the eigenvectors $\mathbf{v}_n$ as columns and $\mathbf{\Lambda}$ is the diagonal matrix of the corresponding eigenvalues λ_n, which are the variances of the data along the principal axes. The contribution of the eigenvector $\mathbf{v}_n$ to the whole data set, normalized to unit variance, is given by the n-th principal component image,

$$\mathbf{y}_n := \lambda_n^{-1/2} \mathbf{v}_n^T \mathbf{X}, \tag{3}$$

where the superscript T denotes the transpose of a vector or matrix. The set $\mathbf{Y}$ of all principal component images is referred to as sphered data set, because the covariance matrix of its column vectors is given by the identity matrix. If the mapping signal is concentrated in the principal components $n_1 \leq n \leq n_2$, a "clean" version $\hat{\mathbf{X}}$ of the data set $\mathbf{X}$ can be calculated using

$$\hat{\mathbf{X}} = \sum_{n=n1}^{n2} \mathbf{v}_n \left(\mathbf{v}_n^T \mathbf{X} \right) = \sum_{n=n1}^{n2} \mathbf{v}_n \lambda_n^{1/2} \mathbf{y}_n. \tag{4}$$

2.4 Extended Spatial Decorrelation

PCA uses variance as the only score for the identification of signal sources. If different sources, such as the mapping signal and some background signal, have similar variances, they cannot be separated by PCA, hence better techniques are needed. In this paragraph we introduce the concept of extended spatial decorrelation (ESD). ESD is applied to the sphered data sets

$\mathbf{Y}$ provided by PCA, in which all information about the variances is removed. In order to complete the separation of signal sources one assumes that the individual source signals are mutually uncorrelated, even if they are shifted relative to each other by a small amount. The autocorrelation function of each source, however, is assumed to be non-vanishing and smooth, corresponding to the assumption of spatial smoothness of each source pattern.

Let the spatial distribution of the n-th source be $\mathbf{s}_n$ with elements $s_{n,\mathbf{r}}$, $n = 1, ..., N$, $\mathbf{r} = (1, ..., P_x, 1, ..., P_y)$, and let $\mathbf{S}$ denote the matrix which contains the N unknown source components as rows. We want to find a separating matrix $\mathbf{W}$ such that the source estimates $\hat{\mathbf{S}} = \mathbf{WY} = \mathbf{W\Lambda^{-1/2}V}^T\mathbf{X}$ have zero cross-correlation functions, i.e. $\langle s_{m,\mathbf{r}} s_{n,\mathbf{r}+\Delta\mathbf{r}} \rangle_{\mathbf{r}} \equiv 0 \; \forall \; \Delta\mathbf{r}$. The matrix $\mathbf{W}$ is orthogonal, because it would otherwise evoke cross-correlations between the source estimates: If $\mathbf{I}$ is the identity matrix, one finds $\mathbf{I} = \hat{\mathbf{S}}\hat{\mathbf{S}}^T = \mathbf{WYY}^T\mathbf{W}^T = \mathbf{WIW}^T = \mathbf{WW}^T$. Following Molgedey and Schuster (Molgedey and Schuster, 1994), the optimal separating matrix based on our assumptions is given by the solution of

$$\frac{1}{2}(\mathbf{G}_{\Delta\mathbf{r}} + \mathbf{G}_{-\Delta\mathbf{r}})\mathbf{W}^{-1} = \mathbf{\Lambda}_{\Delta\mathbf{r}}\mathbf{W}^{-1}, \tag{5}$$

where $G_{mn,\Delta\mathbf{r}} = \langle y_{m,\mathbf{r}} y_{n,\mathbf{r}+\Delta\mathbf{r}} \rangle_{\mathbf{r}}$ is the shifted covariance matrix of the sphered data. The algorithm is very fast (similar to PCA) and can be applied online during the measurement, because it requires only the calculation of two $N \times N$ covariance matrices.

3 Results

Figure 2 demonstrates the removal of a time-dependent artifact from a differential image stack using PCA. The stack was recorded optically from ferret visual cortex using 0 deg and 90 deg oriented stimuli. Figure 2a shows the summed differential image which contains both the mapping signal and a large, roughly annular artifact, which is time-dependent and therefore is still present in the differential image. In figure 2b, the first two principal components, $\mathbf{v}_1$ and $\mathbf{v}_2$, are plotted as time-series. The first principal component has a large variance and a complicated time series, which describes the time-dependence of the artifact, while the second principal component has a smaller variance and a time series which can be interpreted as the time-course of the mapping signal. The corresponding principal component images are given in figures 2c and 2d. They demonstrate that the mapping signal (figure 2d) can be almost completely separated from the time-dependent artifact (figure 2c) by PCA and corroborate the previous interpretation of the time

series. Note, that the separation by PCA was possible, because the artifact and the mapping signal differed strongly in their variances over space and had approximately orthogonal time series. Figure 2c still contains a small fraction of the mapping signal, which is probably due to the presence of white noise and to small deviations of the real time series from orthogonality.

The time series of the global and the mapping signals are both locked to the stimulus. Hence they are probably not orthogonal to each other, and consequently are not separable by PCA. For the separation of the global and the mapping signal using PCA, we generate a combined data stack, which contains several single-condition image stacks for different stimuli in a sequence such as to form a long time series of images. In this combined stack, the global signal shows a similar response irrespective of the stimulus-type, whereas the time-course of the mapping signal depends on the stimulus. Therefore, the time series of both signals are now likely to be nearly orthogonal.

Figure 3 shows the first nine principal component time series (figure 3a), the corresponding principal component images (figure 3b), and the scree-plot (the logarithm of the principal component eigenvalues ordered in size) for a combined data stack, which had been generated by stacking four single-condition image sets ($N = 14$ images each, 8 s stimulus duration, 2 s time between stimuli) for stimuli with orientations 0, 45, 90, and 135 deg and performing first frame analysis. The scree-plot shows that only the first 7-8 principal components carry signals, whereas the higher components, which show roughly uniform variances, carry noise. This agrees with the noisy appearance of the 8th and 9th principal component time series and images. The time-dependences of the first three principal components from top are nearly identical for each stimulus presentation irrespective of the stimulus type. Using their spatial patterns they can be assigned to the global signal (top image) and to signals from larger blood vessels and illumination artifacts (second and third image). The fourth to seventh principal components contain linear combinations of the mapping signals for the different stimulus-conditions, which appear as periodic patterns in the cranial window region of the corresponding images. Note, that PCA cannot separate different single-condition responses from each other, because their variances usually are similar. Thus, it is not useful to assign any biological meaning to the individual principal components that capture the mapping signal.

Signal extraction and noise reduction can be achieved by reconstructing the data set, cf. eq. (4), using only the principal components 4-7. Discarding the higher principal components reduces noise, while discarding the first three principal components removes part of the global signal and the vessel artifacts. Single condition images can be obtained by pixel-wise summation of all resulting images for a given stimulus condition. Figure 4a shows the

0 deg single condition image of the data set of figure 3 before PCA, where both the global signal (diffuse background) and the mapping signal (small dark blobs) are mixed together. Figure 4b displays the reconstruction of the same single-condition image after PCA and noise removal. The global signal is drastically reduced in the reconstruction compared to the original data, whereas the mapping signal is preserved and concentrated. Figure 4c plots the time series $\mathbf{z}$ which results from the back-projection of the pattern $\mathbf{y}$ in figure 4b onto the original data stack: $\mathbf{z} = \mathbf{X}\ \mathbf{y}^T$. It measures, how much of the reconstructed image is contained in each individual frame of the data. The pattern appears only in the first 14 frames, which correspond to the 0 deg stimulus condition. This corroborates that the reconstructed image contains only the 0 deg mapping signal.

The statistical significance level of the mapping signal within each pixel of a single-condition map can be assessed using a linear model (Kay, 1993). The back-projected time series (e.g. the first 14 points of the curve in figure 4c in case of the 0 deg single-condition stack) serve as model functions, the parameters are determined by fitting the linear model to the corresponding cleaned single-condition stack. This procedure provides the minimum-variance unbiased estimator (MVUE) for the strength of the mapping signal within each pixel as well as a measure for its variance. The ratio between the signal strength and its standard deviation defines the Z-score (Mayhew and Zheng, 1996), which serves as a confidence measure for the mapping signal being non-zero. Figure 4d displays the Z-score as a function of space within the region of the cranial window for the 0 deg single condition map of figure 4b. The dark islands in the Z-score mark the regions where the mapping signal significantly differs from zero.

Figure 5 shows the result of an ESD analysis for an individual differential image stack. Figure 5a shows a series of five images of a 0-90 deg differential image stack optically recorded from cat area 17 (time increases from top to bottom). It contains the oscillatory mapping signal that emerges superimposed to a global spatial pattern. Images were low-pass filtered with a cutoff frequency of ($0.54\ \mathrm{mm}^{-1}$) in order to allow the application of ESD (Schießl, Stetter, Mayhew, Askew, McLoughlin, Levitt, Lund and Obermayer, 1999), but no high-pass-filter was applied. Figure 5b lists the three leading principal component images, and figure 5c the conjugate time series obtained from their back-projection. In this series, a movement artifact has been separated (third from bottom), but the mapping signal is still distributed across two images (first and second from bottom) and is still superimposed onto the global background. Figure 5d and 5e display three of the five spatial source patterns and their conjugate time series as estimated by ESD using the shift vector $\Delta\mathbf{r} = (5, 5)$ (the remaining two sources contain noise patterns). Now

the mapping signal is completely concentrated in one source (second from bottom) and is separated from the global pattern (bottom). Figure 5f and 5g contain the conventional differential map and the mapping signal as provided by ESD analysis. A comparison reveals that ESD, in contrast to differential imaging, could remove the global signal and the movement artifact. In figure 5h, finally, the binarized absolute value of the Z-score is given for the map in figure 5g. Black marks regions, in which the absolute value of the Z-score for the middle time series is larger than three.

ESD can also extract the mapping signal from an individual single condition stack. Figure 6a shows a 0 deg single-condition image for the same record as in figure 2. The data set consists of a mixture of the mapping signal, a global background and a time-dependent artifact. Figure 6b shows the best separation result for PCA (top), which is still very poor, and its conjugate time series (bottom). Figure 6c contains the best image (top) and time series (bottom) obtained from ESD. ESD successfully removes the artifact and achieves a strong yet not fully complete separation from the global signal.

Finally, ESD was applied to the same data set as shown in Figure 1 in order to achieve a quantitative comparison of ESD to analysis by bandpass filtering. ESD was performed on lowpass-filtered difference image stacks for different shift vectors with components 0, 5, 10, 15 and 20 pixels. All combinations except the zero shift were used resulting in 24 shift vectors. For each separation result, the source that contained the mapping signal was selected and their signal strength was normalized by back-projection onto the initial image stacks. Then, an orientation map, the orientation histograms, and its first two Fourier components were calculated as for the data in figure 1. All histograms peaked at 0 and 90 deg. The result for the first Fourier component was $a_1 = 0.01 \pm 0.005$ and for the second component $a_2 = 0.11 \pm 0.02$. The errors represent standard deviations for the 24 samples. Because all data originate from the assumption of a single statistical model (namely zero cross-correlation functions between sources), the data can be averaged yielding $a_1 = 0.011 \pm 0.001$ and $a_2 = 0.108 \pm 0.004$ (error is standard error of the mean). In summary, ESD yields a single estimate for the Fourier components. Their variability is due to random noise rather than due to different underlying models, and is much smaller than the systematic variation shown in figure 1.

We have carried out analyses for 10 experiments from 8 cats and ferrets, on which orientation maps have been measured. We find: (i) PCA yielded greatly improved single condition maps compared to standard analysis for 9 out of 10 experiments (experiment 10 did not contain any visible mapping signal and was chosen as an "artifact only" control). ESD led to an improve-

ment in single condition image stacks in 6 data sets. It could not properly treat data sets with large technical artifacts and with a high initial noise level. This is because ESD uses only the information available from an individual single condition stack (as opposed to PCA). (*ii*) In the 9 experiments that contained a mapping signal, the principal components were always arranged as described in figure 4. One of the remaining experiments contained a large technical artifact (probably from a temporal fluctuation in the illumination conditions), which could also be mostly separated from the mapping signal. In contrast to differential imaging, where the mapping signal was not detectable, PCA could extract the signal. (*iii*) We tested variability of the results between different experiments for the same animal on two pairs of experiments each being done for the same animal. Because image contents are translated, rotated and distorted between different experiments, it is difficult to calculate a reliable cross-correlation coefficient between the reconstructed data from both experiments without a sophisticated correction. Visual inspection reveals that the data sets are almost identical up to random noise fluctuations.

4 Discussion

We proposed a new method for the extraction of the mapping signal of optical recordings from other signal components, which are less closely related to stimulated neuronal activity.

If data are analyzed using bandpass-filtering with a given set of cutoff frequencies f_1 and f_2, this corresponds to the statistical model "signals are concentrated within the frequency band $[f_1, f_2]$, the background is concentrated outside". Thus, every pair of cutoff frequencies serves as parameters for the statistical model, which can be arbitrarily chosen. In contrast, the methods proposed in this work are based on parameter-free statistical assumptions, namely "the signals are orthogonal and can be distinguished by variance" (PCA), or "different signal sources are smooth and their cross-correlation functions vanish" (ESD). The shift vector of ESD does not touch the statistical model, i.e. the independence assumption. Rather, the the same kind of independence is assumed for all shift vectors. In particular, this implies that the results obtained for several shifts can be averaged which helps reducing noise.

However, the shift vector for ESD has to be chosen in a range, where both the autocorrelations of the sources and the cross-correlations between the mixtures are large. We chose absolute shifts in the range of half an orientation wavelength. Though only data for $\Delta\mathbf{r} = (5, 5)$ is shown, the

separation results did not change considerably for absolute shifts between 2 and 20 pixels.

We showed that temporal PCA can be successfully used both for noise-reduction and for the removal of global signals and vessel artifacts. Because the global and the mapping signals show a different behavior over space and additionally differ in strength by approximately a factor of 5 (Bonhoeffer and Grinvald, 1996), their variances are strongly different in many cases and they can be separated using PCA. However, this requires application of PCA to a whole sequence of single-condition stacks. In suggesting this mode of application, we extend earlier work (Carmona, Hwang and Frostig, 1995; Cannestra, Blood, Black and Toga, 1996; Everson, Knight and Sirovich, 1997; Everson, Prashanth, Gabbay, Knight, Sirovich and Kaplan, 1998). where PCA has been applied on single condition or differential image stacks. These studies use PCA in order to reduce white noise and to extract prominent prototype time courses of the mixture of intrinsic signals, but different signal components are not separated. However, PCA suffers from the drawbacks that it requires orthogonality of prototype time series, which is not necessarily provided, and that ignores additional sources of knowledge besides the variances of time-series over the data set.

One possibility to overcome this limitation of PCA has been suggested by (Carmona et al., 1995), who combined PCA with wavelet transforms, which performs localized image analysis and thus is sensitive to higher order statistics within the images. In this work we suggest blind source separation by ESD, which does not suffer from the abovementioned drawbacks of PCA. It can complete the separation of the mapping signals from global components and artifacts both in individual differential image stacks and in single-condition stacks, even in cases where the conjugate time-series of different sources are not orthogonal. Let us briefly discuss the assumptions on which ESD is based. Though not proven to be true, smoothness over space is very likely to be given for all signal components. For the mapping and global signals, smoothness is generated by the strong scattering of light within the tissue, which blurs all components over space by at least 100-200 μm (Stetter and Obermayer, 1999). For blood-vessels on the cortical surface, which are continuous structures in one dimension, the autocorrelation functions can extend to more than one millimeter. The assumption of vanishing cross-correlations between the sources is less intuitive, yet in the case of orientation maps, where the mapping signal is oscillatory as opposed to the global signal, the resulting cross-correlation functions between the two patterns are small. Also, we observed that cross-correlations between vessel-patterns, that were extracted from images of the cortex under illumination with green light, and ocular dominance stripes from differential images are

lower than 20 % of the autocorrelations.

While making use of knowledge about spatial coherence, ESD as applied in this work is confined to second order statistics, because it is based on second-order correlation functions. Though this might appear as a limitation, a recent comparison (Schießl et al., 1999) of ESD with Independent Component Analysis (ICA) based on INFOMAX (Bell and Sejnowski, 1995) (moments of any order) and on kurtosis optimization (Hyvärinen and Oja, 1997) (fourth order moments) showed that ESD provides the best separation results for spatially smooth data. This is probably due to the fact that, in the presence of noise, higher order moments are more difficult to estimate using a limited set of data points, than moments of second order. Also, the ICA algorithms usually do not exploit the spatial coherence of patterns as done by ESD.

PCA and ESD are based on fairly general assumptions. However, both methods only work if those assumptions are true, and some care has to be taken when interpreting the results. The only direct test for the biological relevance of both differential maps and PCA/ESD maps is a comparison between the optical maps and the corresponding electrophysiologically measured neuronal response. However, an indirect method for scoring the reconstructed maps pops out of the method: If the spatial neuronal activation patterns have already been characterized, the spatial distributions help identifying the mapping signal (cf., figure 4b), when accompanied by a reasonable conjugate time series (cf., figure 4c). If no information about spatial neuronal activation patterns is available beforehand, the shape of the time-series, which must change coherently with the stimulus onset, can serve as a criterion for the identification of the mapping component. In any case, however, the only direct test for the biological relevance of both differential maps and PCA/ESD maps is a comparison between the optical maps and the corresponding electrophysiologically measured neuronal response.

Acknowledgments

This work has been supported by DFG (OB102/3-1), the Wellcome Trust (050080/Z/97) and the Max Planck Gesellschaft.

References

Amari, S. (1996). Neural learning in structured parameter spaces - natural riemannian gradient., *in* M. C. Mozer, M. I. Jordan and T. Petsche (eds), *Advances in Neural Information Processing Systems*, Vol. 9.

Arieli, A., Sterkin, A., Grinvald, A. and Aertsen, A. (1996). Dynamics of ongoing activity: explanation of the large variability in evoked responses., *Science* **273**: 1868–1871.

Bell, A. J. and Sejnowski, T. J. (1995). An information-maximization approach to blind separation and blind deconvolution., *Neural Comput.* **7**: 1129–1159.

Blasdel, G. G. (1992). Differential imaging of ocular dominance and orientation selectivity in monkey striate cortex., *J. Neurosci.* **12**: 3115–3138.

Bonhoeffer, T. and Grinvald, A. (1996). Optical imaging based on intrinsic signals: The methodology, *in* A. Toga and J. C. Maziotta (eds), *Brain mapping: The methods*, Academic Press, Inc., San Diego, CA, pp. 55–97.

Cannestra, A. F., Blood, A. J., Black, K. L. and Toga, A. W. (1996). The evolution of optical signals in human and rodent cortex., *NeuroImage* **3**: 202–208.

Cardoso, J. F. (1997). Infomax and maximum likelihood for blind source separation, *IEEE Signal Processing Lett.* .

Carmona, R. A., Hwang, W. L. and Frostig, R. D. (1995). Wavelet analysis for brain function imaging, *IEEE Trans. Med. Imaging* **14**: 556–564.

Everson, R., Knight, B. W. and Sirovich, L. (1997). Separating spatially distributed response to stimulation from background. i. optical imaging, *Biol. Cybern.* **77**: 407–417.

Everson, R. M., Prashanth, A. K., Gabbay, M., Knight, B. W., Sirovich, L. and Kaplan, E. (1998). Representation of spatial frequency and orientation in the visual cortex., *Proc. Natl. Acad. Sci.* **95**: 8334–8338.

Grinvald, A., Lieke, E., Frostig, R. D., Gilbert, C. D. and Wiesel, T. N. (1986). Functional architecture of cortex revealed by optical imaging of intrinsic signals., *Nature* **324**: 361–364.

Hyvärinen, A. and Oja, E. (1997). A fast fixed point algorithm for independent component analysis., *Neural Comput.* **9**: 1483–1492.

Jutten, C. and Herault, J. (1986). *Neural Network for Computing*, AIP, New York.

Kay, S. M. (1993). *Fundamentals of statistical signal processing. Estimation theory*, Prentice Hall International EditionsNew Jersey.

Makeig, S., Bell, A. J., Jung, T.-P. and Sejnowski, T. J. (1996). Independent component analysis of electroencephalographic data., *in* D. Touretzky, M. Mozer and M. Hasselmo (eds), *Advances in Neural Information Processing Systems*, MIT Press, Cambridge MA, pp. 145–151.

Mayhew, J. E. W., Askew, S., Zheng, Y., Porril, J., Westby, G. W. M., Redgraves, P., Rector, D. M. and Harper, R. M. (1996). Cerebral vasomotion: 0.1hz oscillation in reflected light imaging of neural activity., *NeuroImage* **4**: 183–193.

Mayhew, J. E. W. and Zheng, Y. (1996). A model for the intrinsic image signal and an evaluation of the methodology of intrisic image signal analysis., *Technical Report 109*, Artificial Intelligence Vision Research Unit AIVRU, University of Sheffield, UK.

McKeown, M., Makeig, S., Brown, G., Jung, T., McKeown, S. J., Makeig, S., Brown, G. G., Jung, T. P., Kindermann, S. S., Bell, A. and Sejnowski, T. (1998). Analysis of fMRI by blind separation into independent spatial components, *Human Brain Mapping* **6**: 160–188.

Molgedey, L. and Schuster, H. G. (1994). Separation of a mixture of independent signals using time delayed correlations, *Phys. Rev. Lett.* **72**: 3634–3637.

Schießl, I., Stetter, M., Mayhew, J. E. W., Askew, S., McLoughlin, N., Levitt, J. B., Lund, J. S. and Obermayer, K. (1999). Blind separation of spatial signal patterns from optical imaging records., *in* J.-F. Cardoso, C. Jutten and P. Loubaton (eds), *Proceedings of the 1. ICA99 Workshop, Aussois*, Vol. 1, pp. 179–184.

Sengpiel, F., Gödecke, I., Strawinski, P., Hübener, M., Löwel, S. and Bonhoeffer, T. (1998). Innate and environmental factors in the formation of functional maps in cat visual cortex., *Neuropharmacology* **37**: 607–621.

Stetter, M. and Obermayer, K. (1999). Simulation of scanning laser techniques for optical imaging of blood-related intrinsic signals., *J. Opt. Soc. Am. A* **16**: in press.

Vetter, R., Vesin, J., Celka, P. and Scherrer, U. (1999). Observer of the autonomic cardiac outflow in humans using non-causal blind source separation., *in* J.-F. Cardoso, C. Jutten and P. Loubaton (eds), *Proceedings of the 1. ICA99-Workshop, Aussois*, pp. 161–166.

Figure Captions:

Figure 1 Biologically relevant quantities which are derived from the orientation map of ferret visual cortex as a function of the cutoff-frequency of an applied high-pass-filter. The diagram plots the number of singularities (solid line) and the first (dash-dotted line) and second (dashed line) Fourier components of the orientation histogram as a function of the cutoff-frequency. The low-pass-cutoff was 2.7 mm^{-1} ($\lambda = 0.37$ mm). Insets show the orientation histograms without high-pass-filtering (left) and after high-pass-filtering (right) with the cutoff-frequency 0.54 mm^{-1} ($\lambda = 1.84$ mm). All quantities depend on the choice of the high-pass cutoff frequency (behavior shown is typical).".

Figure 2 Removal of a time-dependent artifact using PCA. **(a)** Summed differential image ($0 - 90$ deg orientations) recorded from ferret visual cortex. **(b)** The time series of the first (PC 1) and second (PC 2) principal components of the differential image stack. Eigenvalues (variances) were: $\lambda_1 = 45157$, $\lambda_2 = 7489$. **(c)** First and **(d)** second principal component image obtained from the two time series in (b) using eq. (3). Scale bar: 1 mm; the gray scales denote gray values of pixels. Its ranges were determined as the mean $\pm$ three times the standard deviation for each image.

Figure 3 **(a)** The first nine principal component time series and **(b)** the corresponding principal component images, normalized to unit variance, for an image stack from cat area 17 (60d) after combination of four single condition stacks (0,45,90,135 deg) and first-frame analysis (gray scale: ± 3). Legends provide the eigenvalues (variances). The first three components capture the global signal and vessel patterns, whereas the mapping signal is concentrated in components 4-7. **(c)** Logarithm of the eigenvalues sorted by size (scree-plot). All but the first 7-8 principal components contain noise.

Figure 4 Reconstruction of the mapping signal for the data stack of figure 3. **(a)** 0 deg single-condition image after first-frame analysis. **(b)** 0 deg single-condition image for the cleaned data set using principal components 4-7 of figure 3. Scale bars: 1 mm. **(c)** Projection of the reconstructed image (b) onto the raw data. Bar: 0 deg stimulation. **(d)** Z-score for the data in (b). Regions of high significance of the mapping signal are shown in black. Scale bar ranges were determined as the mean $\pm$ three times the standard deviation for each image.

Figure 5 **(a)** Time series of images of a $0 - 90$ deg differential stack from cat area 17 (time interval: 600 ms). Images are low-pass filtered (cutoff: 0.54 mm^{-1}). Scale bar: 1 mm. Gray scale: ± 200. **(b)** Leading three principal component images (bottom = 1. PC; gray scale: ± 400) and **(c)** conjugate

time series for the data set shown in (a). Signal separation is incomplete. **(d)** Estimated spatial source patterns (arbitrary gray scale) and **(e)** conjugate time series after ESD analysis with $\Delta\mathbf{r} = (5, 5)$. The mapping signal is concentrated in the "center" source, and is separated from a global background and a movement artifact. **(f)** Resulting differential map obtained by summation of images in (a) **(g)** Resulting map obtained as the MVUE estimator for the strength of the mapping signal. Model functions were the time series shown in the center and bottom graphs of (e). The global signal and the movement artifact have been successfully removed in this map. **(h)** Significance map for the statistical parameter map in (g). Black indicates regions for which the absolute Z-score was larger than 3.

Figure 6 (a) 0 deg single condition maps after first frame analysis and pixelwise summation. **(b)** Best signal extraction using PCA. Top: principal component image. Bottom: conjugate time series. **(c)** Spatial pattern obtained from ESD analysis (normalized to unit variance). Top: spatial pattern of the source. Bottom: conjugate time series. Images are low-pass filtered (cutoff: 0.54 mm^{-1}). Scale bar: 1 mm.

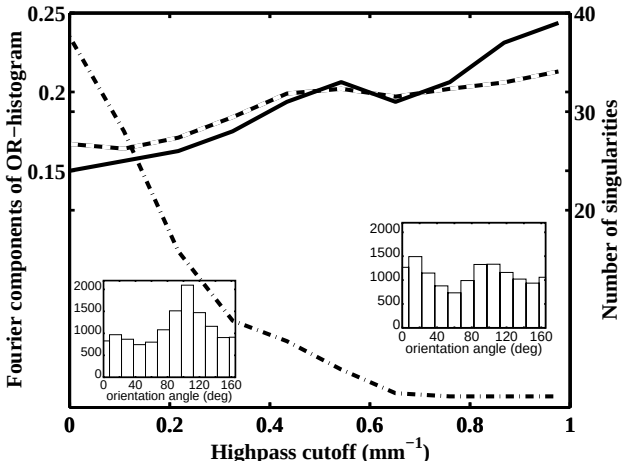

Figure 1 of Stetter et al., ⇑ top, original size.

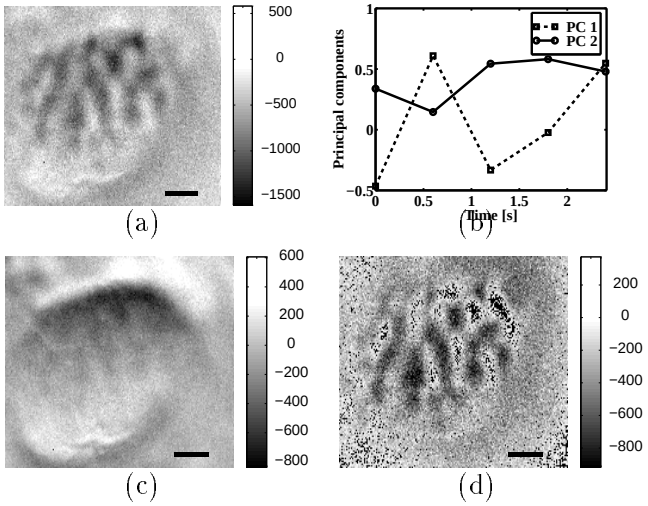

Figure 2 of Stetter et al., ⇑ top, original size.

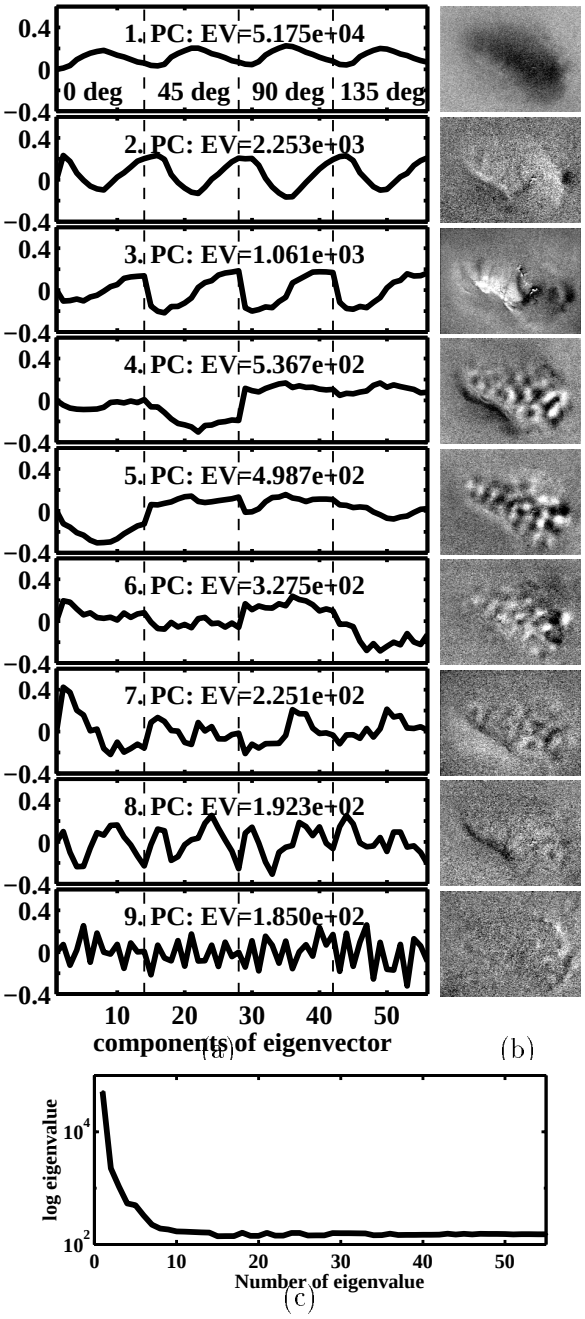

Figure 3 of Stetter et al., ⇑ top, original size.

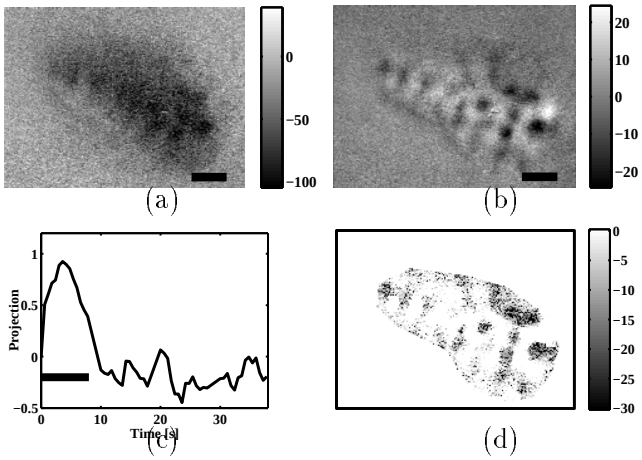

Figure 4 of Stetter et al., ⇑ top, original size.

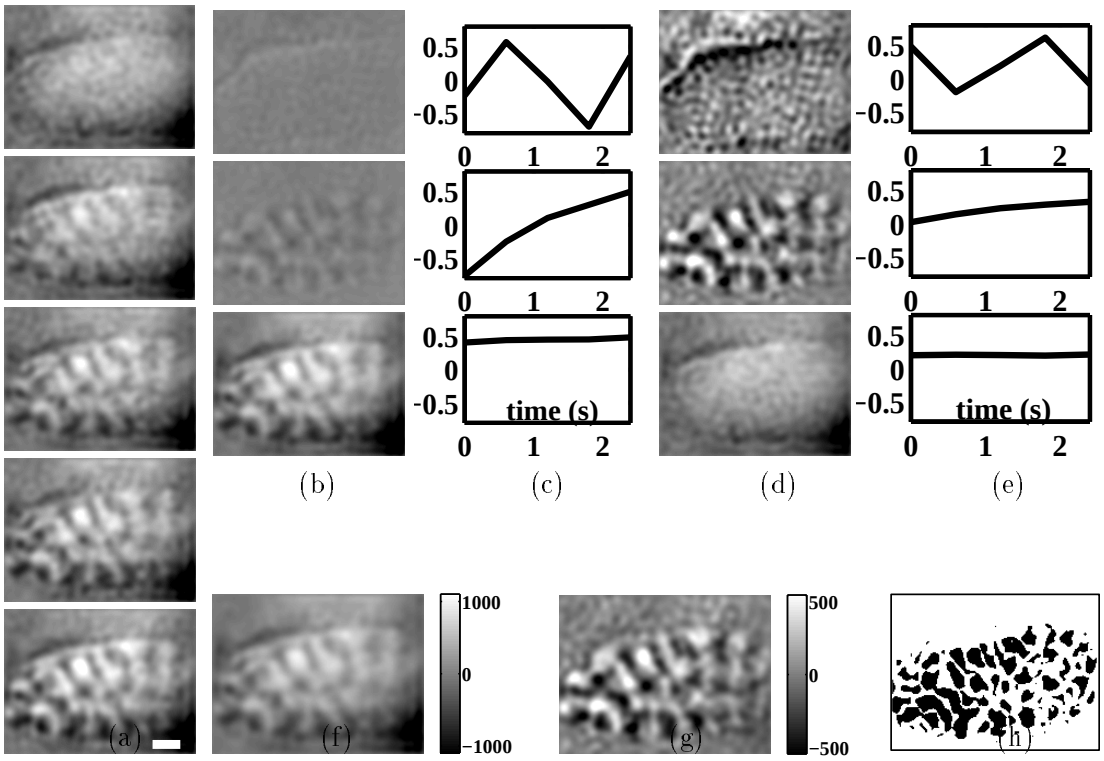

Figure 5 of Stetter et al., ⇑ top, original size.

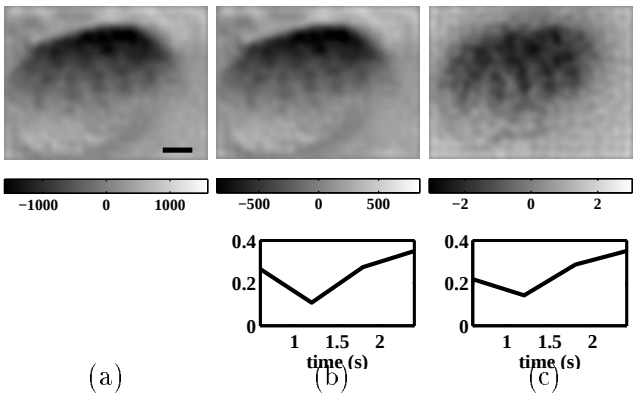

Figure 6 of Stetter et al., ⇑ top, original size.